Hydrol. Earth Syst. Sci., 20, 1703–1717, 2016
www.hydrol-earth-syst-sci.net/20/1703/2016/
doi:10.5194/hess-20-1703-2016

Hydrology and Earth System Sciences
Open Access
EGU

An ice core derived 1013-year catchment-scale annual rainfall reconstruction in subtropical eastern Australia

Carly R. Tozer[1,2], Tessa R. Vance[1], Jason L. Roberts[3,1], Anthony S. Kiem[2], Mark A. J. Curran[3,1], and Andrew D. Moy[3,1]

[1]Antarctic Climate & Ecosystems Cooperative Research Centre, University of Tasmania, Hobart, Tasmania 7001, Australia
[2]Centre for Water, Climate and Land Use, University of Newcastle, Callaghan, NSW 2308, Australia
[3]Australian Antarctic Division, Kingston, Tasmania 7050, Australia

Correspondence to: Carly R. Tozer (carly.tozer@utas.edu.au)

Received: 23 October 2015 – Published in Hydrol. Earth Syst. Sci. Discuss.: 3 December 2015
Revised: 24 March 2016 – Accepted: 11 April 2016 – Published: 11 May 2016

Abstract. Paleoclimate research indicates that the Australian instrumental climate record (∼ 100 years) does not cover the full range of hydroclimatic variability that is possible. To better understand the implications of this on catchment-scale water resources management, a 1013-year (1000–2012 common era (CE)) annual rainfall reconstruction was produced for the Williams River catchment in coastal eastern Australia. No high-resolution paleoclimate proxies are located in the region and so a teleconnection between summer sea salt deposition recorded in ice cores from East Antarctica and rainfall variability in eastern Australia was exploited to reconstruct the catchment-scale rainfall record. The reconstruction shows that significantly longer and more frequent wet and dry periods were experienced in the preinstrumental compared to the instrumental period. This suggests that existing drought and flood risk assessments underestimate the true risks due to the reliance on data and statistics obtained from only the instrumental record. This raises questions about the robustness of existing water security and flood protection measures and has serious implications for water resources management, infrastructure design and catchment planning. The method used in this proof of concept study is transferable and enables similar insights into the true risk of flood/drought to be gained for other paleoclimate proxy poor regions for which suitable remote teleconnected proxies exist. This will lead to improved understanding and ability to deal with the impacts of multi-decadal to centennial hydroclimatic variability.

1 Introduction

Water and catchment management systems (e.g., drought and flood mitigation strategies) and water resources infrastructure have traditionally been designed based on the trends, patterns and statistics revealed in relatively short instrumental climate records (i.e., for Australia usually less than 100 years of data recorded post-1900) (Verdon-Kidd and Kiem, 2010; Ho et al., 2014; Cosgrove and Loucks, 2015; Razavi et al., 2015). This is a concern as Australian paleoclimate research suggests that instrumental climate records are not representative of the true range of hydroclimatic variability possible (Verdon-Kidd and Kiem, 2010; Gallant and Gergis, 2011; Kiem and Verdon-Kidd, 2011; Ho et al., 2014, 2015a, b; Razavi et al., 2015; Vance et al., 2015). For example, paleoclimate archives show evidence of droughts of longer duration than the three major droughts that have affected eastern Australia over the instrumental period – the Federation drought (∼ 1895–1902), World War II drought (∼ 1937–1945) and Millennium or "Big Dry" drought (∼ 1997–2009) (Gergis et al., 2012; Vance et al., 2013; Allen et al., 2015; Vance et al., 2015).

Sources for paleoclimate proxy data include tree rings, coral skeletons, ice cores, speleothems (cave deposits), sediments and documentary evidence (Ho et al., 2014). Ideally, the climate proxy archives are located in the region of interest but in areas where proxy records are sparse or of low resolution, remote proxies are a viable alternative (Ho et al., 2014). Remote proxies exploit circulation teleconnections that link one region to another and are calibrated over

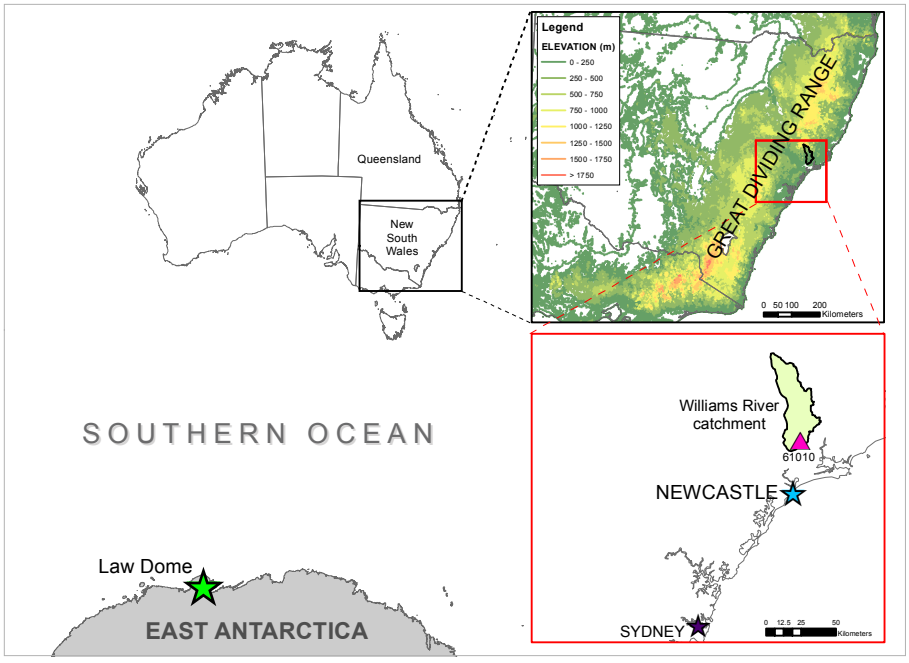

Figure 1. Location of Law Dome in relation to Australia with insets indicating the Great Dividing Range, WR catchment boundary and the location of the 61010 high-quality rainfall gauge, Newcastle and Sydney.

the instrumental period, to develop paleoclimate reconstructions (e.g., rainfall, streamflow) for the target region (e.g., Verdon and Franks, 2007; McGowan et al., 2009; van Ommen and Morgan, 2010; Vance et al., 2013, 2015). When using remote proxies the assumption is that large-scale climate processes driving climate variability at the location of the paleoclimate proxy also drive a high proportion of climate variability at the region of interest (Gallant and Gergis, 2011). For example, van Ommen and Morgan (2010) identified a relationship between precipitation (snowfall) recorded in ice cores from coastal Antarctica and rainfall in southwest Western Australia over the instrumental period, inferring rainfall variability in the region for the past 750 years. Similarly, Lough (2011) found significant correlations between coral luminescence intensity recorded in coral cores from the Great Barrier Reef and summer rainfall variability in northeast Queensland, which enabled the multi-century coral record to be used to reconstruct Queensland summer rainfall back to the 18th century.

Another option is to use the link between large-scale ocean–atmospheric climate processes and climate variability in the region of interest to develop a paleoclimate reconstruction based on a paleoclimate proxy of the climate process. For example, McGowan et al. (2009) reconstructed annual inflows in the Murray River back to 1474 common era (CE) from a reconstruction of the Pacific Decadal Oscillation (PDO) based on the previously identified relationship between the PDO and streamflow in southeastern Australia (e.g., Power et al., 1999a, b; Kiem et al., 2003; Kiem and Franks, 2004; Verdon et al., 2004). A similar approach was also followed by Verdon and Franks (2006, 2007) and Henley et al. (2011).

Vance et al. (2013, 2015) used a hybrid of the approaches discussed above. Vance et al. (2013) developed a millennial length rainfall reconstruction for subtropical eastern Australia by exploiting a relationship between the region's annual rainfall and the summer sea salt record (see Sect. 3) from the Law Dome ice core, East Antarctica (Fig. 1). Of key importance is that the strength of the relationship during the instrumental period (in this case 1889–2009) varies synchronously with the Interdecadal Pacific Oscillation (IPO) (Power et al., 1999a, b), the basin-wide expression of the PDO, with increased correlations found during IPO positive phases (Vance et al., 2013, 2015). The IPO represents decadal sea surface temperature (SST) variability across the Pacific Ocean whereby a positive IPO phase is associated with warming across the tropical Pacific and cooling of the north and south Pacific; the opposite occurs during the negative phase (Power et al., 1999a). The most recent defined complete IPO phases are two positive phases (~ 1924–1941, ~ 1979–1997) and one negative phase (~ 1947–1975) (Power et al., 1999a; Kiem et al., 2003; Kiem and Franks, 2004; Verdon et al., 2004).

Vance et al. (2015) demonstrated that during the IPO negative phase there is a predominantly zonal pressure pattern across the high to mid-latitudes, which switches to a more meridional pattern in IPO positive. Folland et al. (2002) also found that during the IPO positive phase, the mean posi-

tion of the South Pacific Convergence Zone (SPCZ) (usually bounded by Samoa and Fiji) is displaced to the northeast. This northeastern displacement is associated with a more meridional circulation pattern and enhances the link between eastern Australia and mid- to high-latitude climate variability and hence explains the stronger relationship between sea salt recorded at Law Dome and rainfall in eastern Australia during the IPO positive phase. Based on their reconstruction of the IPO, Vance et al. (2015) could therefore identify periods in time (i.e., positive IPO phases) where they had greater confidence in the rainfall reconstruction. A key finding from Vance et al. (2015) was the identification of a century of IPO positive aridity (1102–1212 CE), including evidence of a 39-year drought in southeast Queensland, which is well outside the bounds of instrumental drought duration. This illustrates the importance of investigating climate variability over millennial timescales, particularly in the Southern Hemisphere where many paleoclimate records only span the last 200–500 years (Neukom and Gergis, 2012). Indeed, it is evident that (a) instrumental data are not long enough to allow for meaningful planning for climate variability; (b) paleodata, particularly at the millennial timescale, offers an important insight into the climate beyond the instrumental period; and (c) there is a need to incorporate insights from paleodata into water resources planning and management.

Further work is also required to assess the robustness of the relationship between climate variability in East Antarctica, large-scale climate processes and eastern Australia, a region with limited local paleoclimate proxy data (Vance et al., 2013; Ho et al., 2014). Practical usefulness of the insights provided by the paleoclimate reconstructions for water resources management at the catchment scale also requires investigation. Therefore, the links between the Law Dome sea salt record, eastern Australian rainfall and the IPO are further explored in this paper through the development of a millennial length, annual resolution and catchment-scale rainfall reconstruction for the Williams River (WR) catchment (Fig. 1). The WR catchment is located on the eastern seaboard of New South Wales, east of the Great Dividing Range (Fig. 1). The eastern seaboard contains about half of Australia's population, and a proportionate amount of economic infrastructure and activity. The region has hydroclimate features that are distinct from the rest of Australia (e.g., Verdon and Franks, 2005; Timbal, 2010) and lacks high-resolution paleoclimate proxies (Ho et al., 2014). This means there is significant vulnerability, uncertainty and knowledge gaps relating to flood and drought risk in eastern Australia. This recognition has recently motivated the development of the Eastern Seaboard Climate Change Initiative (ESCCI), to better understand the causes and impacts of current and future climate-related risk in the region (http://www.climatechange.environment.nsw.gov.au/About-climate-change-in-NSW/Evidence-of-climate-change/Eastern-seaboard-climate-change-initiative). The WR catchment is of particular regional importance because it forms part of the conjunctive-use headworks scheme for potable water supply to ∼ 600 000 people in Newcastle, the sixth largest residential region in Australia (Kiem and Franks, 2004; Mortazavi-Naeini et al., 2015).

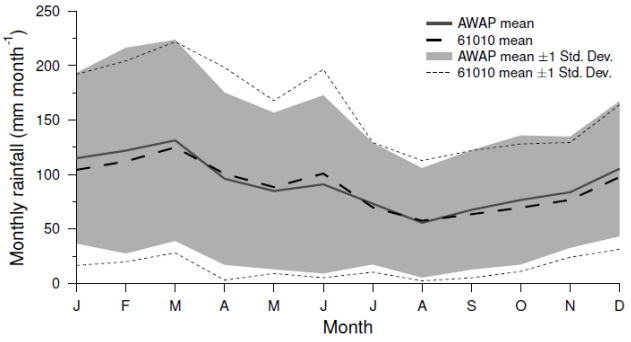

Figure 2. Climatology of WR catchment rainfall. Shown is the mean and standard deviation of monthly rainfall recorded at the 61010 gauge and for the AWAP catchment average.

In the following sections we present a description of the WR catchment location and relevant climate data, including a discussion of the link between Law Dome, East Antarctica and eastern Australia. We proceed with an investigation into the relationship between summer sea salts from Law Dome and rainfall in the WR catchment and follow with the development of a 1013-year catchment-scale rainfall reconstruction (based on the Law Dome sea salt record) and discussion of the insights and implications emerging from this reconstruction.

2 Rainfall variability in the Williams River catchment

For the calibration data in this study we used daily 5 km × 5 km gridded rainfall data obtained from the Australian Water Availability Project (AWAP) (Jones et al., 2009) for the period 1900–2010. The AWAP grid cells overlapping the WR catchment were extracted and used to calculate catchment average monthly rainfall totals for the WR catchment. Due to known biases and uncertainty associated with gridded climate data (e.g., Tozer et al., 2012), the AWAP-based information was ground-truthed with data from a high-quality (Lavery et al., 1997) rainfall gauge (61010) located within the WR catchment. The highest and most variable rainfall in the WR catchment is received from December to May (summer and autumn) (Fig. 2) and the hydrological water year for the WR catchment is therefore defined as October to September in order to encompass this high rainfall period (pers. comm., Brendan Berghout, Senior Water Resources Engineer, Hunter Water Commission).

Rainfall variability in the WR catchment is influenced by the Great Dividing Range to the west (Fig. 1), which provides orographic enhancement and the Tasman Sea to the east, which brings moisture to the region (Pepler et al., 2014).

Synoptic scale influences known as East Coast Lows (ECLs), marine or continental low-pressure systems, which tend to develop in the Tasman Sea, are responsible for much of the extreme weather (e.g., heavy rainfall, high winds) recorded in eastern New South Wales (Speer et al., 2009; Browning and Goodwin, 2013; Pepler et al., 2014b; Ji et al., 2015; Kiem et al., 2015; Twomey and Kiem, 2015). Indeed, ECLs have been found to contribute 20–30 % of annual rainfall in the WR region (Pepler et al., 2014a). In addition to these local influences several large-scale ocean–atmospheric processes influence rainfall in the WR catchment (e.g., Kiem and Franks, 2001, 2004; Risbey et al., 2009). The El Niño–Southern Oscillation (ENSO) and IPO have been related to interannual to multi-decadal variability in both WR rainfall and runoff (Kiem and Franks, 2001, 2004). Drier (wetter) catchment conditions typically occur during El Niño (La Niña) events and the IPO modulates both the frequency and magnitude of ENSO impacts such that drought risk is increased during IPO positive phases and flood risk is increased during IPO negative phases (Kiem and Franks, 2001, 2004; Kiem et al., 2003; Kiem and Verdon-Kidd, 2013). Indian Ocean SSTs are also known to influence eastern Australian rainfall during winter and spring (Verdon and Franks, 2005; Risbey et al., 2009).

In addition, the subtropical ridge (STR) and Southern Annular Mode (SAM) impact rainfall variability in the eastern seaboard (e.g., Risbey et al., 2009; Ho et al., 2012; Whan et al., 2013). A positive SAM phase has been related to increased daily rainfall in summer and spring (Hendon et al., 2007; Risbey et al., 2009) while variability in the position of the STR is significantly correlated with rainfall in the eastern seaboard. That is, a shift south of the STR is associated with increased rainfall in the region (Timbal, 2010; Whan et al., 2013). Variability in the intensity of the STR is also related to rainfall variability in the eastern seaboard though to a lesser extent than variability in the STR position (Timbal, 2010).

3 The Law Dome–eastern Australia rainfall proxy

3.1 Law Dome ice core site details

Law Dome is a small, coastal icecap located in Wilkes Land, East Antarctica (Fig. 1), and the site of the Dome Summit South (DSS) ice core, which spans around 90 000 years (Roberts et al., 2015). DSS has high annual snowfall of around 0.63 m (water equivalent), which allows for a monthly resolution record in the upper portion of the core and highly accurate dating (van Ommen and Morgan, 1997; Vance et al., 2013; Roberts et al., 2015). The ice core was dated by counting annual layers with known volcanic horizons used to establish dating accuracy (Plummer et al., 2012). As a result, the Law Dome record was dated with absolute accuracy from 1807 to 2009 CE and with ±1-year error from 894 to 1807 CE. The sea salt record used here was produced using trace ion chromatography from 2.5 to 5 cm sub-samples of the ice cores (Curran et al., 1998; Palmer et al., 2001). The Law Dome summer (December–March) sea salts (LD_{SSS}) were extracted from the full record and used by Vance et al. (2013) and Vance et al. (2015) as a rainfall proxy for eastern Australia. Here we use a slightly extended LD_{SSS} record to cover the epoch 1000–2012 CE using the improved composite record of Roberts et al. (2015).

3.2 The link between sea salt deposition at Law Dome and large-scale ocean–atmospheric processes

The climate signals recorded in the Law Dome ice core are driven by large-scale ocean–atmospheric processes rather than local factors (Bromwich, 1988; Delmotte et al., 2000; Masson-Delmotte et al., 2003; Vance et al., 2013). The southern Indian Ocean is the main source of moisture delivered to Law Dome (Delmotte et al., 2000; Masson-Delmotte et al., 2003) and sea salt deposition is related to the mid-latitude westerly winds (associated with the SAM) in the Indian and Pacific sectors of the Southern Ocean (Goodwin et al., 2004; Vance et al., 2015). Seasonal to annual scale SST anomalies in the equatorial Pacific are known to propagate to high southern latitudes (Karoly, 1989; Mo and Higgins, 1998; Ding et al., 2012). The resulting circumpolar geopotential height and zonal wind anomalies influence the SAM (L'Heureux and Thompson, 2006), and ultimately deliver sea salt aerosols to coastal Antarctica (Vance et al., 2013). Indeed, Vance et al. (2013) found a significant correlation between ENSO-related SST variability in the central-western equatorial Pacific and LD_{SSS}, with low summer sea salt years associated with El Niño events over the period 1889-2009. Furthermore, spectral analysis of the 1010-year LD_{SSS} record found significant ($p < 0.01$) spectral features in the 2–7-year ENSO band. Similar to the LD_{SSS} rainfall proxy discussed previously, the LD_{SSS} ENSO proxy varies decadally, coherent with the IPO, with a stronger relationship during IPO positive phases (Vance et al., 2013, 2015).

It is thus clear that the ocean–atmospheric processes associated with sea salt deposition at Law Dome (e.g., IPO, ENSO, SAM and variability in the Indian Ocean) are the same as those that influence rainfall variability in the WR catchment (discussed in Sect. 2). We can therefore expect LD_{SSS} to explain some variability in the rainfall in the WR catchment.

4 Investigating the relationship between LD_{SSS} and rainfall in the Williams River catchment

Vance et al. (2013) found a relationship between LD_{SSS} and the prior January–December rainfall west of the Great Dividing Range. The region of interest in this study is further south and east of the Great Dividing Range, so we needed to re-evaluate if this temporal offset was appropri-

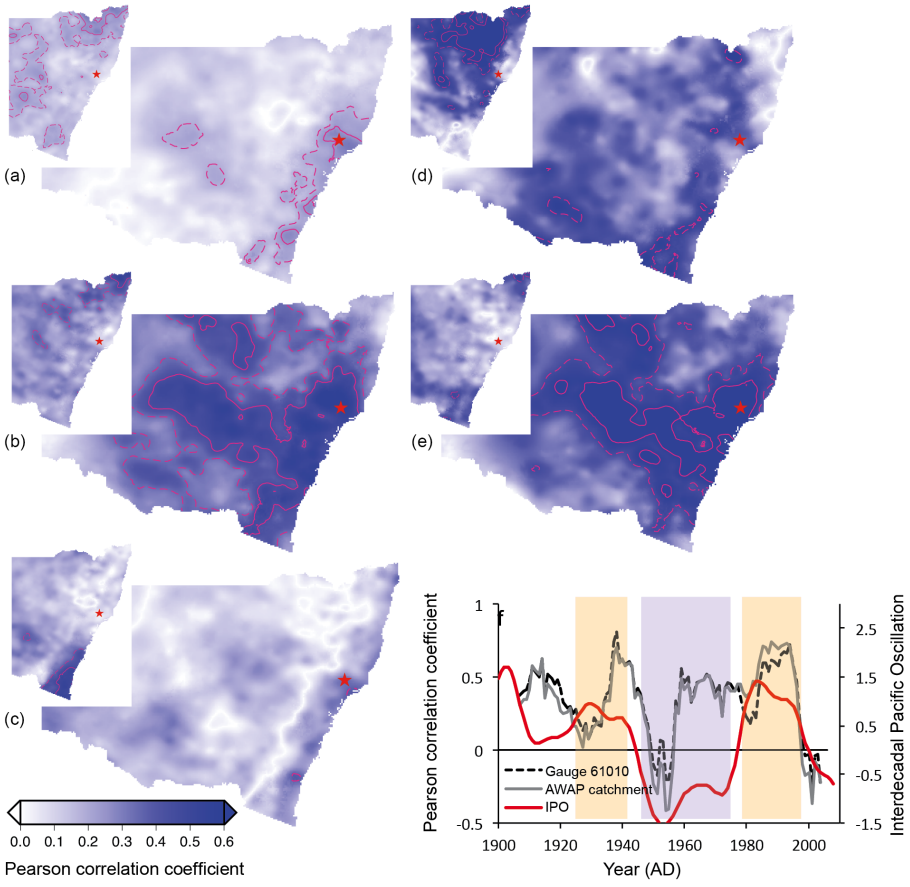

Figure 3. Correlations between **(a)** 12-month average (October–September) AWAP rainfall and LD_{SSS} for the 1900–2010 period with inset showing correlations between annual AWAP rainfall calculated from January–December and LD_{SSS} for 1900–2010 period, **(b)** as in **(a)** but for the combined IPO positive phases (1924–1941, 1979–1997), **(c)** as in **(a)** but for the IPO negative phase (1947–1975), **(d)** as in **(a)** but for the first IPO positive (1924–1941) phase **(e)** as in **(a)** but for the second IPO positive (1979–1997) phase and **(f)** 13-year moving window correlations between 12-month average (October–September) rainfall recorded at gauge 61010 and the AWAP WR catchment average and LD_{SSS} with shading indicating IPO positive (yellow) and IPO negative (purple) phases (red line shown indicates 13-year smoothed instrumental IPO record). Note that for **(a–e)** the star represents the location of the WR catchment centroid, dashed pink line shows 99 % significance level.

ate. This re-evaluation was via a damped least-squares regression between AWAP grid-cell data and the LD_{SSS} record using the Marquardt–Levenberg method, a method capable of multi-variate and non-linear regression. Although it was only used for uni-variate linear regression here, the method was selected for compatibility with planned future work. For every AWAP grid cell in New South Wales, we performed linear least-squares regression between the LD_{SSS} record and 12-month-averaged rainfall over a 24 month lead/lag range centered about the summer sea salt period (December–March). The regression coefficients for each lead/lag were used to generate an estimated spatial rainfall time series. The Pearson correlation coefficient between the estimated rainfall and AWAP rainfall for each grid cell was then assessed for each lead/lag. This process allowed us to determine the seasonal window for rainfall that optimized the WR rainfall–LD_{SSS} relationship in order to optimize the utility of the LD_{SSS} record.

From the lead/lag analysis, October–September and November–October annual rainfall in the region encompassing the WR catchment was found to have the highest and most spatially coherent relationship with LD_{SSS}. We present the October–September rainfall / LD_{SSS} correlations (Fig. 3) as this period also corresponds to the water year in the Newcastle region (discussed in Sect. 2) and hence all further analysis is based on the 12-month rainfall totals calculated from October–September.

Figure 3 shows spatial maps of the magnitude of the correlations between October–September WR rainfall and LD_{SSS} for the 1900–2010 (i.e., October 1900–September 2010) period as well as subsets for the different IPO phases. For comparison Fig. 3a–e are inset with maps for the January–December rainfall / LD_{SSS} correlations, the analysis period

Table 1. Pearson correlation values between LD_{SSS} and 12-month average (October–September) rainfall recorded at gauge 61010 and the AWAP WR catchment average for the 1900–2010 period and IPO phases. Bootstrap 95 % confidence intervals are also indicated (Mudelsee, 2003). Bold values are significant at 95 %.

Time period	61010	AWAP catchment average
Full record (1900–2010)	**0.29** [0.12–0.45]	**0.28** [0.10–0.44]
IPO positive (1924–1941, 1979–1997)	**0.47** [0.23–0.66]	**0.55** [0.31–0.73]
IPO positive (1924–1941)	**0.33** [0.01–0.59]	0.34 [−0.11–0.68]
IPO positive (1979–1997)	**0.59** [0.23–0.81]	**0.67** [0.44–0.82]
IPO negative (1947–1975)	**0.37** [0.13–0.57]	**0.32** [0.06–0.54]

used in Vance et al. (2013) and Vance et al. (2015). Figure 3f indicates the 13-year moving window correlations between LD_{SSS} and October–September for rainfall recorded at gauge 61010 and the AWAP WR catchment average in order to identify low frequency variability associated with the IPO. The Pearson correlation coefficients between LD_{SSS} and October–September annual rainfall recorded at gauge 61010 and the AWAP WR catchment average for the full record and IPO phases are presented in Table 1. The significance of the relationships are confirmed using bootstrap confidence intervals based on the method of Mudelsee (2003).

The insets of Fig. 3a–e reveal low correlations in the WR catchment region. The highest correlations occur in inland New South Wales and into southeastern Queensland, the focus region of Vance et al. (2013) and Vance et al. (2015). However, when the correlation is aligned with the WR catchment water year (October–September) we see a shift in the region of significant correlation (Fig. 3a) to coastal New South Wales and, in particular, large parts of the eastern seaboard. Importantly, correlations significant at the 99 % level are seen over the WR catchment region. Rainfall at gauge 61010 and AWAP catchment average show significant correlations with LD_{SSS} (Pearson correlation coefficients of 0.29 and 0.28 respectively) over the 1900–2010 period (Table 1).

As expected, based on the results of Vance et al. (2013, 2015) (discussed in Sect. 3), the strength of the correlation between October–September rainfall and LD_{SSS} varies decadally. Figure 3b–c indicate that the relationship between the variables is stronger during the IPO positive phases relative to the negative phase. Figure 3d–e and the results in Table 1, however, suggest that although the relationship between October–September rainfall and LD_{SSS} is stronger in IPO positive phase, this increase in strength relative to IPO negative and the full record (1900–2010) is primarily due to the very high correlation in the second IPO positive phase (1979–1997). In fact, the correlation between rainfall recorded at gauge 61010 and LD_{SSS} during the IPO negative phase is greater than the correlation in the first IPO positive phase (Table 1). Figure 3f further highlights that an increase (decrease) in the strength of the LD_{SSS}–WR rainfall relationship is not always synchronous with IPO positive (negative) phases.

This result appears to be in contrast to Vance et al. (2013, 2015), who found a clear link between IPO phase, LD_{SSS} and January–December rainfall in southeast Queensland and northeastern New South Wales (west of the Great Dividing Range). That is, the correlation between these variables was poor during the IPO negative phase, yet was significant for both positive phases. Vance et al. (2013, 2015) used calendar year rainfall as opposed to a more catchment specific analysis period used in this study. Another key difference is that the focus region here is further south, on the coast and under the orographic influence of the Great Dividing Range. Furthermore, although interdecadal and interannual tropical Pacific Ocean variability (e.g., ENSO and IPO) has been found to impact the whole of Australia at various times of the year (e.g., Power et al., 1999a; Risbey et al., 2009), the amount of rainfall variability explained by these processes reduces to the south while climate mechanisms stemming from the mid- to high latitudes (e.g., SAM and the STR, discussed in Sect. 2) increase their influence on rainfall variability (Risbey et al., 2009).

In addition, as mentioned previously, around one-quarter of annual rainfall received in the WR catchment results from ECLs (Pepler et al., 2014a). In 1950 and 1955, the Newcastle region experienced heavy rainfall and floods as a result of severe ECLs (Callaghan and Helman, 2008; Callaghan and Power, 2014) and indeed eastern Australia in general was subject to an increase in intense storm activity between the 1940s and 1970s (Power and Callaghan, 2015). The relationship between LD_{SSS} and rainfall in the WR catchment could not be expected to hold during these short duration but intense local-scale weather events and remote proxy records in general are usually incapable of resolving events like these. As such, this period of elevated intense storm activity may explain the marked reduction (and change of sign) in the correlation between LD_{SSS} and rainfall in the WR catchment in the early 1950s (Fig. 3f). ECL variability has been related to the IPO, with Speer (2008) finding that during the second IPO positive phase (i.e., 1979–1997) there was a decrease in ECLs relative to IPO negative. This would correspond to a reduction in ECL-related rainfall over New South Wales in

the most recent IPO positive phase and is further evidence that these short duration, chaotic events affect the relationship between LD_{SSS} and rainfall in the WR catchment.

Indeed, a better understanding of the role of ECLs and also the relative influence of ENSO, IOD, SAM, STR and other large-scale processes on rainfall in the WR catchment (as is currently being investigated as part of the ESCCI project) will undoubtedly improve our understanding of the variability in the strength of the LD_{SSS}–WR rainfall teleconnection. It should also be noted that one of the key difficulties in understanding the non-stationarity in the climate of the Southern Hemisphere is the lack of quality atmospheric/oceanic data in the Southern Ocean in the pre-1979 satellite era, particularly in the Indian/West Pacific sector. It is likely that more high-resolution ice core records from the Indian Ocean sector of East Antarctica will assist in filling this data gap (Vance et al., 2016). Underpinning the above issue is that variability in the Australian climate record can be up to centennial scale, which cannot be resolved using relatively short instrumental data sets (Gallant et al., 2013). Ultimately, for the purposes of this initial reconstruction, we have assumed stationarity in the LD_{SSS}–Williams River rainfall relationship.

5 Reconstructing rainfall in the Williams River catchment

5.1 Development of the Williams River rainfall reconstruction

The linear regression coefficients determined for the full 1900–2010 instrumental calibration period (Sect. 4) were applied to the 1000–2012 CE LD_{SSS} data to produce 1013 years of rainfall data for each AWAP grid cell in the WR catchment. This grid-cell data were then spatially averaged to produce a WR catchment average rainfall reconstruction time series.

5.2 Comparing the catchment-average rainfall reconstruction with instrumental (AWAP) data

A comparison between the AWAP catchment average and reconstructed WR catchment rainfall over the instrumental period (1900–2010) is presented in Fig. 4. The instrumental mean and pattern of peaks and troughs in the recorded rainfall is well represented in the reconstruction but the range of variability is underestimated. While the magnitude of the extremes is important, the key focus is that the reconstruction captures the duration and timing of wet and dry periods. The thinking behind this is that a short, but extreme (in terms of rainfall deficit) drought, for example, will have less severe implications on water security in a catchment than a drought of long duration with consistently below average (but not necessarily extremely below average) rainfall. Encouragingly, periods post-1900 that are known to be associated with droughts and flooding in the WR catchment are identified in the reconstruction, e.g., the World War II drought in the late 1930s, the Millennium drought in the 1990s to 2000s and the flood dominated 1950s and 1960s (e.g., Verdon-Kidd and Kiem, 2009; Gallant et al., 2012; Callaghan and Power, 2014).

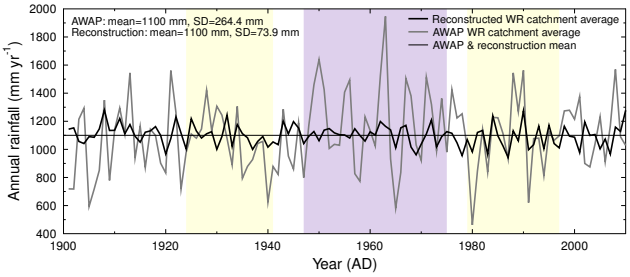

Figure 4. Reconstructed rainfall (thick black), AWAP WR catchment average rainfall (grey) and reconstruction/AWAP mean rainfall (thin black). Shading indicates IPO positive (yellow) and IPO negative (purple) phases.

The rainfall reconstruction captures around 10 % of the rainfall variability in the WR catchment for the full 1900–2010 instrumental period (Table 1). In terms of IPO phases, it is clear that the reconstruction is in better agreement with the instrumental record for the most recent IPO positive phase (1979–1997) relative to the first IPO positive phase and the IPO negative phase. This is no surprise given the higher correlation between LD_{SSS} and Williams River rainfall in the recent IPO positive period, i.e., LD_{SSS} variability captures around 40 % of the Williams River rainfall variability (Table 1). Influences on the stationarity of the LD_{SSS}–WR rainfall relationship were discussed in Sect. 4.

Table 2 presents the root mean square error (RMSE) and reduction in error (RE) between the rainfall reconstruction and 12-month average (October–September) rainfall recorded at gauge 61010 and the AWAP WR catchment average for the 1900–2010 period and IPO phases. An RE value greater than zero indicates that the reconstruction is skillful and has better predictive skill than climatology (Cook, 1992). While improved RMSE and RE statistics were recorded for the most recent IPO positive (1979–1997) relative to the first IPO positive and IPO negative phases, it is clear that the reconstruction has skill across the 1900–2010 instrumental period. For the full instrumental record, the reconstruction has an RMSE of around 25 % of the annual instrumental rainfall with an RE value greater than zero.

5.3 A millennial rainfall reconstruction for the WR catchment

Figure 5 presents the 1013-year rainfall reconstruction produced for the WR catchment. From the 10-year smoothed record it is evident that there have been multi-year periods of either above or below average rainfall. A multi-century dry

Table 2. Root mean square error in mm year^{-1} (%) and reduction in error between the rainfall reconstruction and 12-month average (October–September) rainfall recorded at gauge 61010 and the AWAP WR catchment average for the 1900–2010 period and IPO phases.

Time period	61010		AWAP catchment average	
	RMSE mm (%)	RE	RMSE mm (%)	RE
Full record (1900–2010)	267 (25.1)	0.07	254 (23.1)	0.08
IPO positive (1924–1941, 1979–1997)	239 (22.5)	0.14	202 (18.4)	0.25
IPO positive (1924–1941)	254 (23.9)	0.10	187 (17.0)	0.08
IPO positive (1979–1997)	223 (21.0)	0.11	216 (19.6)	0.33
IPO negative (1947–1975)	254 (23.9)	0.10	306 (27.8)	0.02

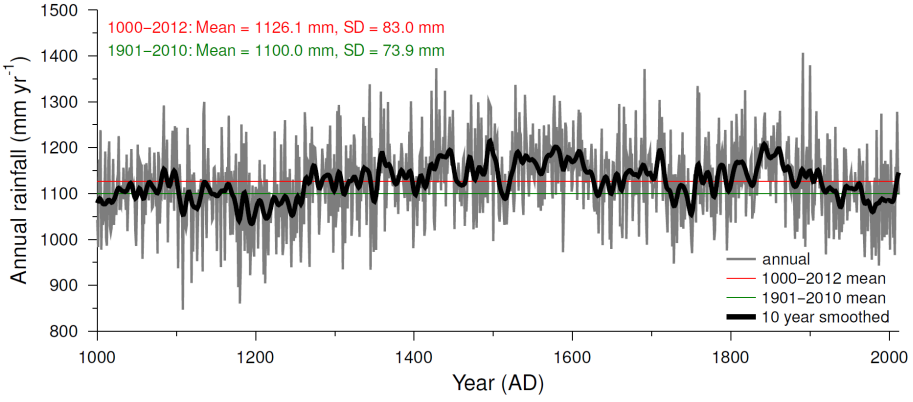

Figure 5. WR catchment rainfall reconstruction (grey line), 10-year Gaussian smooth (bold black line) mean of the rainfall reconstruction for 1000–2012 period (red line) and 1900–2010 period (green line).

period is evident from around 1100 to 1250 CE, while two similarly persistent wet periods are seen from around 1400 to 1600 and 1800 to 1900 CE.

As mentioned previously, few rainfall proxy records exist in eastern Australia. Those that do tend to be outside of the eastern seaboard region in climate regimes that have significant differences, cover different time periods or are at varying (lower) resolutions, which limits the ability to compare them to the reconstruction provided here. However, broad commonalities can be discussed. Heinrich et al. (2009) developed a 154-year rainfall reconstruction for Brisbane, located near the northern boundary of the eastern seaboard, from red cedar tree-ring analysis. Since the record commences in 1854, which is within the instrumental period for the Brisbane region (Heinrich et al., 2009), the utility of this record for comparison here is limited. Nevertheless, the authors found drier periods in the 1880s, 1900–1920, most of 1940s and 1990s and wetter periods in the 1860s, 1890s, 1930s and 1970s, which fits with the results shown in Fig. 5 if the reconstruction is compared with the instrumental mean as opposed to the full 1000–2012 mean. Although not a rainfall reconstruction, an aridity index of wet and dry periods is available based on speleothems from the Wombeyan Caves, located in the Sydney region (i.e., within the eastern seaboard) for the 749 BCE to 2001 CE period (McDonald, 2005; McDonald et al., 2009, 2013). Dry epochs evident in the Wombeyan aridity index, for the period where it overlaps with the WR reconstruction, include late 1100s, around 1500, mid-1700s and early 1900s, which is consistent with the WR reconstruction illustrated in Fig. 5. Similarly, the Wombeyan record indicates epochs that were "not dry" include the early 1400s, 1510-1600, early 1700s, and late 1800s, which is again consistent with the results presented in Fig. 5 (McDonald, 2005; McDonald et al., 2009, 2013; Ho et al., 2015a, b).

In addition, Gergis et al. (2012) produced a multi-proxy based annual rainfall reconstruction for a broad southeastern portion of Australia for the 1783–1988 CE period, finding the 20th century to be drier during their ∼200-year analysis period. Similarly, Fig. 5 shows that the recent era (1900–present) is relatively dry in the post-1783 time period and also in the context of the last 1000 years, though it is not unprecedented. For the 1685–1981 CE period, Lough (2011) found drier and less variable summer rainfall in far northeastern Queensland between 1760 and 1850 and a tendency for a wetter climate from the mid-1850s to 1900 from their coral-based rainfall proxy. Likewise, the reconstruction shown here tends to indicate a drier period post-1700, switching to a wetter regime from the late-1700s to the beginning of the 20th century.

Table 3. Duration of longest dry and wet periods for the AWAP and reconstructed rainfall.

Mean (mm) used to determine wet/dry	SD (mm) used to determine wet/dry	x value used to determine wet/dry (Threshold = mean $- x \times$ SD)	Duration longest dry period (years)	Dry period	Duration of of longest wet period (years)	Wet period
(a) AWAP catchment average rainfall (1900–2010)						
1100.0 (1900–2010)	264.6 (1900–2010)	0 (mean)	8	1935–1942	5	1927–1931
		0.1	8	1935–1942	8	1925–1932
		0.2	8	1935–1942	8	1925–1932
		0.3	8	1935–1942	8	1925–1932
		0.4	8	1935–1942	9	1948–1956
		0.5	9	1979–1987	9	1924–1932, 1948–1956, 1971–1979
(b) Reconstructed rainfall (1900–2010)						
1100.0 (1900–2010)	73.9 (1900–2010)	0 (mean)	7	1936–1942	7	1907–1913
		0.1	7	1936–1942	8	1907–1914
		0.2	8	1935–1942	10	1905–1914
		0.3	8	1935–1942	10	1905–1914
		0.4	9	1973–1981	10	1905–1914
		0.5	11	1973–1983	10	1905–1914
(c) Reconstructed rainfall (1000–2012)						
1100.0 (1900–2010)	73.9 (1900–2010)	0 (mean)	7	1936–1942	16	1590–1605, 1834–1849
		0.1	9	1215–1223	26	1831–1856
		0.2	9	1215–1223	27	1830–1856
		0.3	12	1193–1204	39	1830–1868
		0.4	12	1193–1204	39	1830–1868
		0.5	12	1193–1204, 1212–1223	39	1830–1868
(d) Reconstructed rainfall (1000–2012)						
1126.1 (1000–2012)	83.0 (1000–2012)	0 (mean)	12	1193–1204	16	1834–1849
		0.1	12	1193–1204	16	1834–1849
		0.2	12	1193–1204	16	1834–1849
		0.3	17	1117–1133	16	1590–1605, 1834–1849
		0.4	17	1117–1133	26	1831–1856
		0.5	18	1206–1223	27	1830–1856

Ultimately we find good agreement with existing nearby rainfall reconstructions. This further validates the rainfall reconstruction presented here particularly in light of previously identified concerns with comparing it to other reconstructions in the eastern Australia region.

5.4 Implications for water resources management

While Fig. 5 gives insights into periods of above and below average rainfall, of particular interest for hydrological studies and water resources management is not only whether a year or sequence of years is above or below the long-term average but also whether a multi-year or multi-decadal epoch is generally wet or dry even though some years within that epoch may be slightly below or above the long-term average. For example, a year that is only 0.1 standard deviations above the average is unlikely to provide enough rainfall to break a drought or fill reservoirs. To account for this, we define "wet" and "dry" years as (Eq. 1):

$$\begin{aligned} &\text{wet} = \text{years where rainfall} > \text{mean} - x \times \text{SD}, \\ &\text{dry} = \text{years where rainfall} < \text{mean} + x \times \text{SD}. \end{aligned} \quad (1)$$

For example, for a standard deviation (SD) of 0.1 (and annual average of 1100 mm), the range is 1092.6–1107.4 mm.

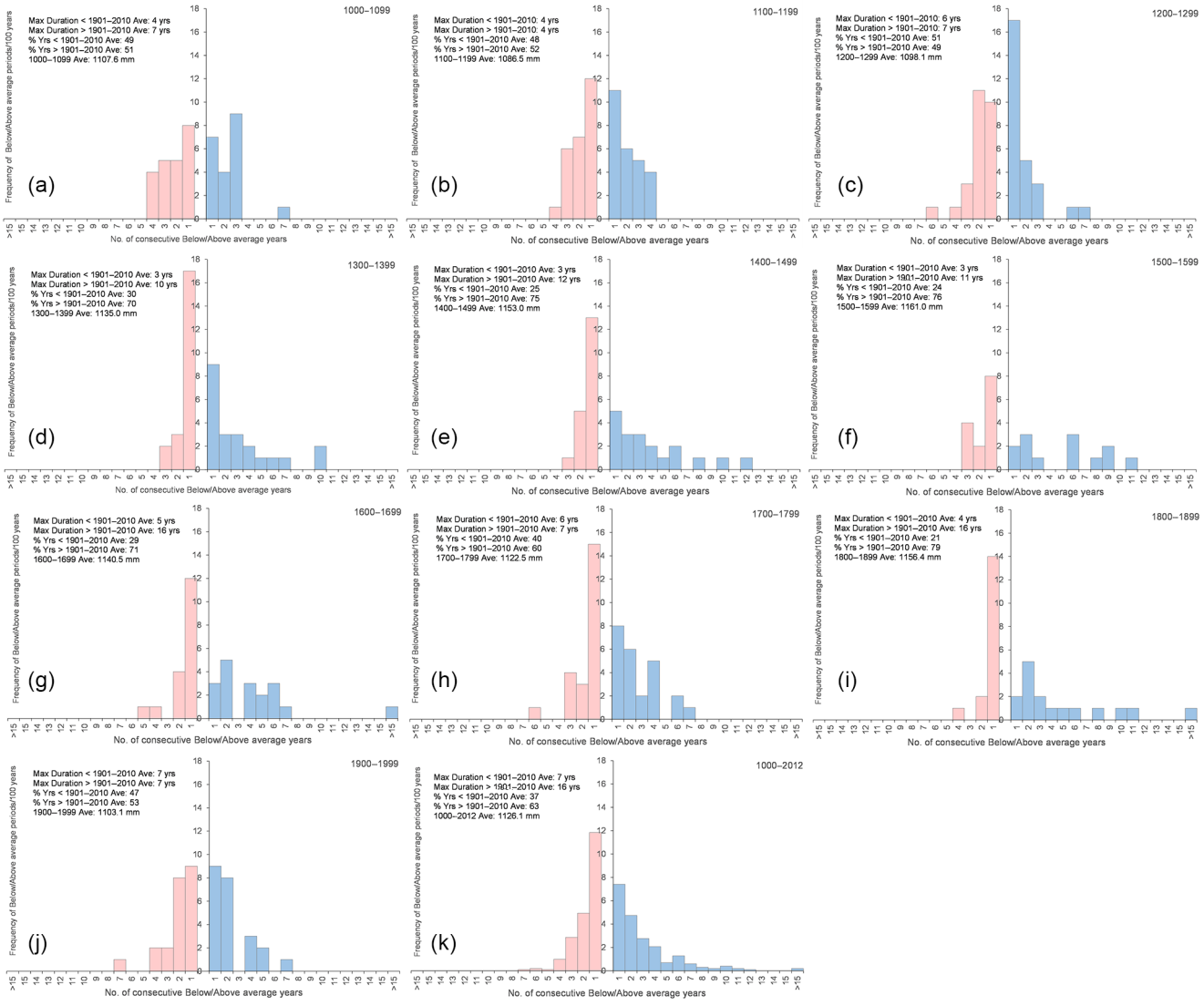

Figure 6. Histograms of duration of above (blue) and below (pink) average rainfall periods in each century since CE 1000. **(a)**–**(j)** are centennial subsets and **(k)** is the CE 1000–2012 period (note different axis scaling). Above/below average are defined using $x = 0$ in Eq. (1) (as per Table 2).

That is, a wet year will be defined as any year with annual rainfall greater than 1092.6 mm and a dry year as any year with annual rainfall less than 1107.4 mm. Some years will be defined as both "wet" and "dry" but this methodology avoids a situation where a consistently wet (or dry) period is broken by a single year that is slightly below (or above) the mean.

Table 3 compares the persistence of the longest above and below average rainfall periods ($x = 0$ in Eq. 1), and "wet/dry" periods ($x = 0.1$, 0.2, 0.3, 0.4, 0.5 in Eq. 1) in the AWAP catchment average rainfall and the reconstruction. Note that the time periods identified in Table 3 should be considered in light of the ± 1 year dating uncertainty of the LD_{SSS} record discussed in Sect. 3.1. As shown in Table 3a and b, the reconstruction captures the dry periods, in terms of duration and timing, of the AWAP instrumental record well and also the duration of the longest wet periods. However, the timing of the wettest periods detected by the reconstruction is different to that seen in the AWAP record. As previously discussed this is likely due to the inability of the LD_{SSS} reconstruction to characterize extreme local-scale synoptic activity in the WR region (i.e., ECLs). Importantly, this also implies that the wettest epochs in the reconstruction may be an underestimation, as the reconstruction is least accurate during wet periods caused predominantly by local-scale influences (e.g., ECLs). In other words, wet periods associated with increased ECL activity (e.g., similar to the 1950s) are possible and the magnitude of rainfall associated with these events would be

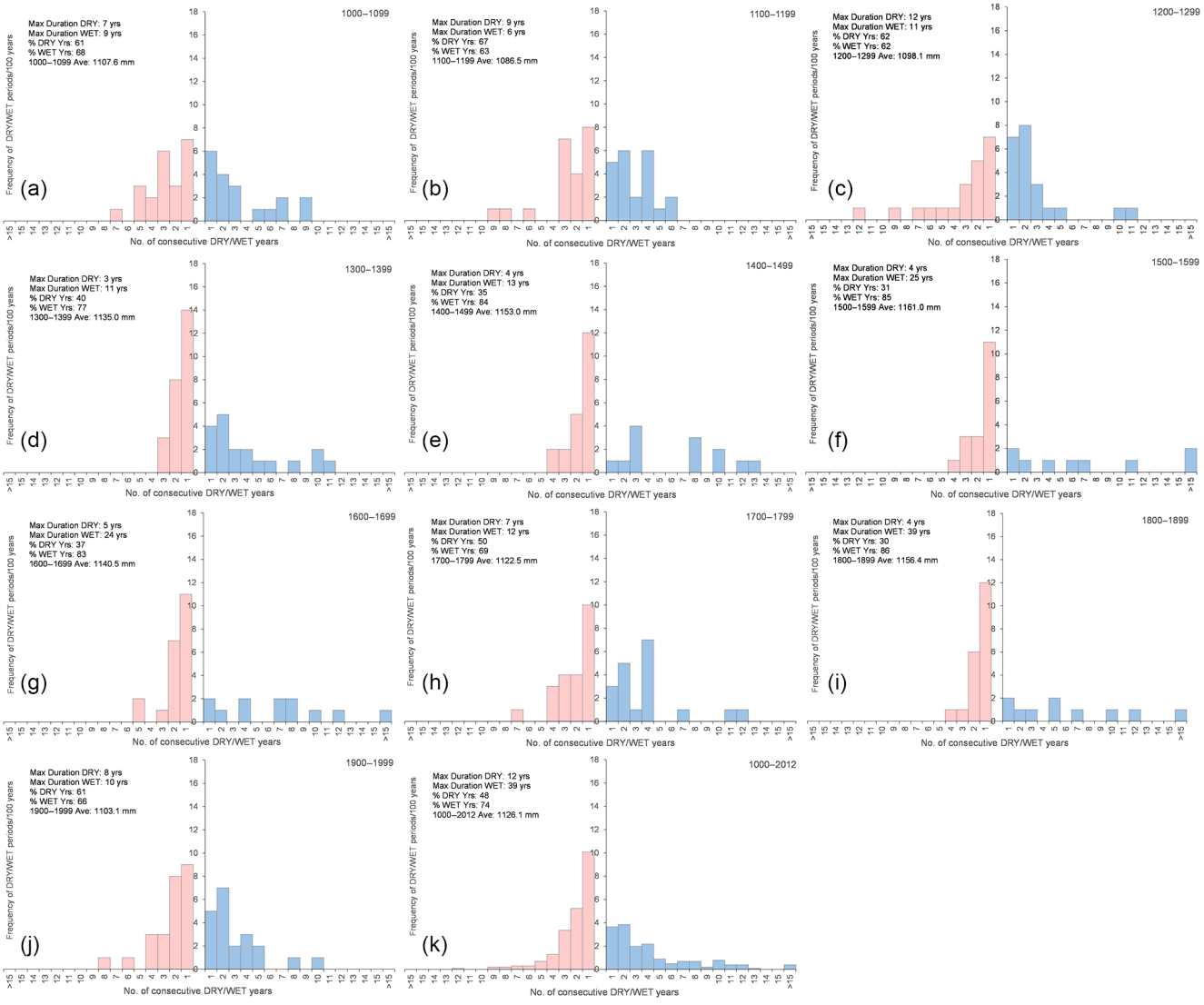

Figure 7. Histograms of duration of WET (blue) and DRY (pink) average periods during each century since CE 1000. **(a)**–**(j)** are centennial subsets and **(k)** is the CE 1000–2012 period (note different axis scaling). WET/DRY are defined using $x = 0.3$ in Eq. (1) (as per Table 2).

over and above the preinstrumental wet epochs suggested by the LD_{SSS} reconstruction.

Figure 6 shows the duration of above and below average rainfall periods during each century since 1000 CE (and also for the whole 1013-year reconstruction period, panel k). To easily visualize the results, Fig. 6 combines all durations > 15 years (information on all durations is included in Table S1 in the Supplement). Figure 6 clearly shows that (a) some centuries are drier (more pink) than others (more blue) and (b) the most recent complete century (1900–1999, panel j), where the majority of our instrumental record comes from, is not representative of either the duration or frequency of periods of above or below average rainfall experienced pre-1900.

While the results in Fig. 6 are important, of greater interest is the identification of the persistence of wet or dry periods even though some years within the otherwise dry (wet) regime were slightly wetter (drier) than average. Table 3a and b show that for varying x values in Eq. (1) the duration of the longest wet or dry periods in the instrumental period does not markedly change. If dry and wet epochs, defined relative to the 1100.0 mm instrumental mean are extracted from the preinstrumental reconstruction, a different story emerges (Table 3c). For a standard deviation threshold of 0.3, for example, the results show that the longest dry epochs persist for up to 12 years instead of a maximum of 8 years post-1900, while wet epochs have lasted almost 5 times as long (maximum of 39 years preinstrumental compared to a maximum of 8 years in the instrumental period). A similar result is observed if

the full reconstruction mean (1126.1 mm) is used to indicate wet or dry (Table 3d), with both the dry and wet epochs persisting up to twice as long in the preinstrumental compared to the instrumental period. Figure 7 (and the associated Tables S2 and S3) further illustrates this point (and the points made in relation to Fig. 6) by clearly showing that the proportion, frequency and duration of wet/dry epochs in the instrumental period (1900–1999) is not representative of either the overall situation throughout the last 1000 years or the situation in any century pre-1900. Also of interest is that some centuries tend to have short dry periods compared with long dry periods and vice versa – e.g., the 15th and 16th century (Fig. 7e and f) compared to the 12th and 13th century (Fig. 7b and c). The same can be said for wet periods. The variation in the distribution of dry/wet-period duration between centuries further suggests that water resources management and planning based on the statistics of 100 years of data (or less) is problematic.

6 Conclusions

This study produced a 1013-year rainfall reconstruction for the WR catchment, a location without any local paleoclimate proxies. The strength of the relationship between LD_{SSS} and annual WR rainfall was found to vary decadally but, unlike Vance et al. (2013, 2015), was not always coherent with the IPO. This is likely due to the different climate regime that the coastal WR catchment is subject to (e.g., likely more influence from mid-latitude processes) compared to the previous studies, which were located further north and predominantly west of the Great Dividing Range. The WR catchment is also strongly influenced by local-scale coastal storms such as ECLs, which may provide an explanation for the different relationship to the IPO, as well as the breakdown in the East Antarctic–WR teleconnection in periods associated with increased ECL activity (e.g., the 1950s).

Despite the acknowledged non-stationarity in the relationship (which is being further investigated in ongoing research) the relationship between LD_{SSS} and rainfall in the WR catchment is significant over the full 1900–2010 calibration period and indeed the reconstruction shows skill across this period. The reconstruction was found to agree well with identified dry/wet periods in other rainfall reconstructions in the eastern Australia region providing further validation. Ultimately, the LD_{SSS}-based reconstruction shows that the instrumental period ($\sim$ 1900–2010) is not representative of the proportion, frequency or duration of wet/dry epochs in any century in the preinstrumental era. This is consistent with recent independent studies focussed on Tasmania (Allen et al., 2015) and the Murray-Darling Basin (Ho et al., 2015a, b).

These findings provide compelling evidence that existing hydroclimatic risk assessment and associated water resources management, infrastructure design, and catchment planning in the WR catchment is flawed given the reliance on drought and flood statistics derived from post-1900 information. Figure 3 (and Fig. 4a in Vance et al., 2015) suggests that the same is true for most of eastern Australia and indeed may also be the case for other regions in Australia that are identified as (or yet to be identified as) having similar teleconnections with East Antarctica, e.g., southwest Western Australia (van Ommen and Morgan, 2010). Therefore, the robustness of existing flood and drought risk quantification and management in eastern Australia is questionable and the insights from paleoclimate data need to be incorporated into catchment planning and management frameworks, especially given the multi-decadal and centennial hydroclimatic variability demonstrated in this study.

Acknowledgements. This work was supported by the Australian Government's Cooperative Research Centres Programme through the Antarctic Climate and Ecosystems Cooperative Research Centre (ACE CRC). The Australian Antarctic Division provided funding and logistical support for the DSS ice cores (AAS projects 4061 and 4062). The Centre for Water, Climate and Land Use at the University of Newcastle provided partial funding for Tozer's salary.

Edited by: D. Mazvimavi

References

Allen, K. J., Nichols, S. C., Evans, R., Cook, E. R., Allie, S., Carson, G., Ling, F., and Baker, P. J.: Preliminary December–January inflow and streamflow reconstructions from tree rings for western Tasmania, southeastern Australia, Water Resour. Res., 51, 5487–5503, doi:10.1002/2015WR017062, 2015.

Bromwich, D. H.: Snowfall in high southern latitudes, Rev. Geophys., 26, 149–168, doi:10.1029/RG026i001p00149, 1988.

Browning, S. A. and Goodwin, I. D.: Large-scale influences on the evolution of winter subtropical maritime cyclones affecting Australia's east coast, Mon. Weather Rev., 141, 2416–2431, doi:10.1175/MWR-D-12-00312.1, 2013.

Callaghan, J. and Helman, P.: Severe storms on the east coast of Australia 1770–2008, Griffith Centre for Coastal Management, Griffith University, Southport, Australia, 2008.

Callaghan, J. and Power, S.: Major coastal flooding in southeastern Australia 1860–2012, associated deaths and weather systems, Austr. Meteorol. Oceanogr. J., 64, 183–213, 2014.

Cook, E. R.: Using tree rings to study past El Nino/Southern Oscillation influences on climate, in: El Nino: historical and paleoclimatic aspects of the southern oscillation, edited by: Diaz, H. F. and Markgraf, V., Cambridge University Press, Cambridge, UK, New York, NY, USA, 476 pp., 1992.

Cosgrove, W. J. and Loucks, D. P.: Water management: current and future challenges and research directions, Water Resour. Res., 51, 4823–4839, doi:10.1002/2014WR016869, 2015.

Curran, M. A. J., van Ommen, T. D., and Morgan, V.: Seasonal characteristics of the major ions in the high-accumulation Dome Summit South ice core, Law Dome, Antarctica, in: Annals of Glaciology, edited by: Budd, W. F., Int. Glaciological Soc., Cambridge, 27, 385–390, 1998.

Delmotte, M., Masson, V., Jouzel, J., and Morgan, V. I.: A seasonal deuterium excess signal at Law Dome, coastal eastern Antarctica: a southern ocean signature, J. Geophys. Res.-Atmos., 105, 7187–7197, doi:10.1029/1999JD901085, 2000.

Ding, Q., Steig, E. J., Battisti, D. S., and Wallace, J. M.: Influence of the Tropics on the Southern Annular Mode, J. Climate, 25, 6330–6348, doi:10.1175/JCLI-D-11-00523.1, 2012.

Folland, C. K., Renwick, J. A., Salinger, M. J., and Mullan, A. B.: Relative influences of the Interdecadal Pacific Oscillation and ENSO on the South Pacific Convergence Zone, Geophys. Res. Lett., 29, 21-1–21-4, doi:10.1029/2001GL014201, 2002.

Gallant, A. J. E. and Gergis, J.: An experimental streamflow reconstruction for the River Murray, Australia, 1783–1988, Water Resour. Res., 47, W00G04, doi:10.1029/2010WR009832, 2011.

Gallant, A. J. E., Kiem, A. S., Verdon-Kidd, D. C., Stone, R. C., and Karoly, D. J.: Understanding hydroclimate processes in the Murray-Darling Basin for natural resources management, Hydrol. Earth Syst. Sci., 16, 2049–2068, doi:10.5194/hess-16-2049-2012, 2012.

Gergis, J., Gallant, A., Braganza, K., Karoly, D., Allen, K., Cullen, L., D'Arrigo, R., Goodwin, I., Grierson, P., and McGregor, S.: On the long-term context of the 1997–2009 "Big Dry" in South-Eastern Australia: insights from a 206-year multiproxy rainfall reconstruction, Climatic Change, 111, 923–944, doi:10.1007/s10584-011-0263-x, 2012.

Goodwin, I. D., van Ommen, T. D., Curran, M. A. J., and Mayewski, P. A.: Mid latitude winter climate variability in the South Indian and southwest Pacific regions since 1300 AD, Clim. Dynam., 22, 783–794, doi:10.1007/s00382-004-0403-3, 2004.

Heinrich, I., Weidner, K., Helle, G., Vos, H., Lindesay, J., and Banks, J. C. G.: Interdecadal modulation of the relationship between ENSO, IPO and precipitation: insights from tree rings in Australia, Clim. Dynam., 33, 63–73, doi:10.1007/s00382-009-0544-5, 2009.

Hendon, H. H., Thompson, D. W. J., and Wheeler, M. C.: Australian Rainfall and Surface Temperature Variations Associated with the Southern Hemisphere Annular Mode, J. Climate, 20, 2452–2467, doi:10.1175/jcli4134.1, 2007.

Henley, B. J., Thyer, M. A., Kuczera, G., and Franks, S. W.: Climate-informed stochastic hydrological modeling: incorporating decadal-scale variability using paleo data, Water Resour. Res., 47, W11509, doi:10.1029/2010WR010034, 2011.

Ho, M., Kiem, A. S., and Verdon-Kidd, D. C.: The Southern Annular Mode: a comparison of indices, Hydrol. Earth Syst. Sci., 16, 967–982, doi:10.5194/hess-16-967-2012, 2012.

Ho, M., Verdon-Kidd, D. C., Kiem, A. S., and Drysdale, R. N.: Broadening the spatial applicability of paleoclimate information – a case study for the Murray–Darling Basin, Australia, J. Climate, 27, 2477–2495, doi:10.1175/JCLI-D-13-00071.1, 2014.

Ho, M., Kiem, A. S., and Verdon-Kidd, D. C.: A paleoclimate rainfall reconstruction in the Murray–Darling Basin (MDB), Australia: 1. Evaluation of different paleoclimate archives, rainfall networks, and reconstruction techniques, Water Resour. Res., 51, 8362–8379, doi:10.1002/2015WR017058, 2015a.

Ho, M., Kiem, A. S., and Verdon-Kidd, D. C.: A paleoclimate rainfall reconstruction in the Murray–Darling Basin (MDB), Australia: 2. Assessing hydroclimatic risk using paleoclimate records of wet and dry epochs, Water Resour. Res., 51, 8380–8396, doi:10.1002/2015WR017059, 2015b.

Ji, F., Evans, J., Argueso, D., Fita, L., and Di Luca, A.: Using large-scale diagnostic quantities to investigate change in East Coast Lows, Clim. Dynam., 45, 2443–2453, doi:10.1007/s00382-015-2481-9, 2015.

Jones, D. A., Wang, W., and Fawcett, R.: High-quality spatial climate data-sets for Australia, Austr. Meteorol. Oceanogr. J., 58, 233–248, 2009.

Karoly, D. J.: Southern Hemisphere circulation features associated with El Niño–Southern Oscillation Events, J. Climate, 2, 1239–1252, doi:10.1175/1520-0442(1989)002<1239:shcfaw>2.0.co;2, 1989.

Kiem, A. S. and Franks, S. W.: On the identification of ENSO-induced rainfall and runoff variability: a comparison of methods and indices, Hydrolog. Sci. J., 46, 1–13, 2001.

Kiem, A. S. and Franks, S. W.: Multi-decadal variability of drought risk, eastern Australia, Hydrol. Process., 18, 2039–2050, doi:10.1002/hyp.1460, 2004.

Kiem, A. S. and Verdon-Kidd, D. C.: Steps toward "useful" hydroclimatic scenarios for water resource management in the Murray-Darling Basin, Water Resour. Res., 47, W00G06, doi:10.1029/2010WR009803, 2011.

Kiem, A. S. and Verdon-Kidd, D. C.: The importance of understanding drivers of hydroclimatic variability for robust flood risk planning in the coastal zone, Austr. J. Water Resour., 17, 126–134, 2013.

Kiem, A. S., Franks, S. W., and Kuczera, G.: Multi-decadal variability of flood risk, Geophys. Res. Lett., 30, 1035, doi:10.1029/2002GL015992, 2003.

Kiem, A. S., Twomey, C. R., Lockart, N., Willgoose, G. R., and Kuczera, G.: The impact of East Coast Lows (ECL) on eastern Australia's hydroclimate – do we need to consider sub-categories of ECLs?, 36th Hydrology and Water Resources Symposium, Hobart, Australia, 7–10 December, 2015.

L'Heureux, M. L. and Thompson, D. W. J.: Observed Relationships between the El Niño–Southern Oscillation and the Extratropical Zonal-Mean Circulation, J. Climate, 19, 276–287, doi:10.1175/JCLI3617.1, 2006.

Lavery, B., Joung, G., and Nicholls, N.: An extended high-quality historical rainfall dataset for Australia, Aust. Meteorol. Mag., 46, 27–38, 1997.

Lough, J. M.: Great Barrier Reef coral luminescence reveals rainfall variability over northeastern Australia since the 17th century, Paleoceanography, 26, PA2201, doi:10.1029/2010PA002050, 2011.

Masson-Delmotte, V., Delmotte, M., Morgan, V., Etheridge, D., van Ommen, T., Tartarin, S., and Hoffmann, G.: Recent southern Indian Ocean climate variability inferred from a Law Dome ice core: new insights for the interpretation of coastal Antarctic isotopic records, Clim. Dynam., 21, 153–166, doi:10.1007/s00382-003-0321-9, 2003.

McDonald, J.: Climate Controls on Trace Element Variability in Cave Drip Waters and Calcite: A Modern Study from Two Karst Systems in S.E. Australia, School of Environment and Life Sciences, University of Newcastle, Newcastle, Australia, 2005.

McDonald, J., Drysdale, R., Hodge, E., Hua, Q., Fischer, M. J., Treble, P. C., Greig, A., and Hellstrom, J. C.: One thousand year palaeohydrological record derived from SE Australian stalagmites, EGU General Assembly 2009, Vienna, 2009, 11554, 2009.

McDonald, J., Drysdale, R., Hua, Q., Hodge, E., Treble, P. C., Greig, A., Fallon, S., Lee, S., and Hellstrom, J. C.: A 1500 year

southeast Australian rainfall record based on speleothem hydrological proxies, AMOS Annual Conference 2013 – Sense and Sensitivity, Melbourne, Australia, 11–13 February, 2013.

McGowan, H. A., Marx, S. K., Denholm, J., Soderholm, J., and Kamber, B. S.: Reconstructing annual inflows to the headwater catchments of the Murray River, Australia, using the Pacific Decadal Oscillation, Geophys. Res. Lett., 36, L06707, doi:10.1029/2008GL037049, 2009.

Mo, K. C. and Higgins, R. W.: The Pacific–South American Modes and Tropical Convection during the Southern Hemisphere Winter, Mon. Weather Rev., 126, 1581–1596, doi:10.1175/1520-0493(1998)126<1581:TPSAMA>2.0.CO;2, 1998.

Mortazavi-Naeini, M., Kuczera, G., Kiem, A. S., Cui, L., Henley, B., Berghout, B., and Turner, E.: Robust optimization to secure urban bulk water supply against extreme drought and uncertain climate change, Environ. Modell. Softw., 69, 437–451, doi:10.1016/j.envsoft.2015.02.021, 2015.

Mudelsee, M.: Estimating Pearson's correlation coefficient with bootstrap confidence interval from serially dependent time series, Math. Geol., 35, 651–665, doi:10.1023/B:MATG.0000002982.52104.02, 2003.

Neukom, R. and Gergis, J.: Southern Hemisphere high-resolution palaeoclimate records of the last 2000 years, Holocene, 22, 501–524, doi:10.1177/0959683611427335, 2012.

Palmer, A. S., van Ommen, T. D., Curran, M. A. J., Morgan, V., Souney, J. M., and Mayewski, P. A.: High-precision dating of volcanic events (AD 1301–1995) using ice cores from Law Dome, Antarctica, J. Geophys. Res.-Atmos., 106, 28089–28095, doi:10.1029/2001JD000330, 2001.

Pepler, A., Coutts-Smith, A., and Timbal, B.: The role of East Coast Lows on rainfall patterns and inter-annual variability across the East Coast of Australia, Int. J. Climatol., 34, 1011–1021, doi:10.1002/joc.3741, 2014a.

Pepler, A., Di Luca, A., Ji, F., Alexander, L. V., Evans, J. P., and Sherwood, S. C.: Impact of identification method on the inferred characteristics and variability of Australian East Coast Lows, Mon. Weather Rev., 143, 864–877, doi:10.1175/MWR-D-14-00188.1, 2014b.

Plummer, C. T., Curran, M. A. J., van Ommen, T D., Rasmussen, S. O., Moy, A. D., Vance, T. R., Clausen, H. B., Vinther, B. M., and Mayewski, P. A.: An independently dated 2000 yr volcanic record from Law Dome, East Antarctica, including a new perspective on the dating of the 1450s CE eruption of Kuwae, Vanuatu, Clim. Past, 8, 1929–1940, doi:10.5194/cp-8-1929-2012, 2012.

Power, S. B., and Callaghan, J.: Variability in severe coastal flooding in south-eastern Australia since the mid-19th century, associated storms and death tolls, J. Appl. Meteorol. Climatol., doi:10.1175/JAMC-D-15-0146.1, online first, 2015.

Power, S., Casey, T., Folland, C., Colman, A., and Mehta, V.: Inter-decadal modulation of the impact of ENSO on Australia, Clim. Dynam., 15, 319–324, doi:10.1007/s003820050284, 1999a.

Power, S., Tseitkin, F., Mehta, V., Lavery, B., Torok, S., and Holbrook, N.: Decadal climate variability in Australia during the twentieth century, Int. J. Climatol., 19, 169–184, doi:10.1002/(sici)1097-0088(199902)19:2<169::aid-joc356>3.0.co;2-y, 1999b.

Razavi, S., Elshorbagy, A., Wheater, H., and Sauchyn, D.: Toward understanding nonstationarity in climate and hydrology through tree ring proxy records, Water Resour. Res.,51, 1813–1830, doi:10.1002/2014WR015696, 2015.

Risbey, J. S., Pook, M. J., McIntosh, P. C., Wheeler, M. C., and Hendon, H. H.: On the remote drivers of rainfall variability in Australia, Mon. Weather Rev., 137, 3233–3253, 2009.

Roberts, J., Plummer, C., Vance, T., van Ommen, T., Moy, A., Poynter, S., Treverrow, A., Curran, M., and George, S.: A 2000 year annual record of snow accumulation rates for Law Dome, East Antarctica, Clim. Past, 11, 697–707, doi:10.5194/cp-11-697-2015, 2015.

Speer, M. S.: On the late twentieth century decrease in Australian east coast rainfall extremes, Atmos. Sci. Lett., 9, 160–170, 2008.

Speer, M. S., Wiles, P., and Pepler, A.: Low pressure systems off the New South Wales coast and associated hazardous weather: establishment of a database, Austr. Meteorol. Oceanogr. J., 58, 29–39, 2009.

Timbal, B.: The climate of the Eastern Seaboard of Australia: a challenging entity now and for future projections, IOP Conference Series: Earth and Environmental Science, Canberra, Australia, 27–29 January 2010, 11, 012013, 2010.

Tozer, C. R., Kiem, A. S., and Verdon-Kidd, D. C.: On the uncertainties associated with using gridded rainfall data as a proxy for observed, Hydrol. Earth Syst. Sci., 16, 1481–1499, doi:10.5194/hess-16-1481-2012, 2012.

Twomey, C. R. and Kiem, A. S.: Spatial analysis of Australian seasonal rainfall anomalies and their relation to East Coast Lows on the Eastern Seaboard of Australia, 36th Hydrology and Water Resources Symposium, Hobart, Australia, 7–10 December, 2015.

van Ommen, T. D. and Morgan, V.: Calibrating the ice core paleothermometer using seasonality, J. Geophys. Res.-Atmos., 102, 9351–9357, doi:10.1029/96JD04014, 1997.

van Ommen, T. D., and Morgan, V.: Snowfall increase in coastal East Antarctica linked with southwest Western Australian drought, Nature Geosci., 3, 267–272, doi:10.1038/ngeo761, 2010.

Vance, T. R., van Ommen, T. D., Curran, M. A. J., Plummer, C. T., and Moy, A. D.: A millennial proxy record of ENSO and Eastern Australian rainfall from the Law Dome ice core, East Antarctica, J. Climate, 26, 710–725, doi:10.1175/JCLI-D-12-00003.1, 2013.

Vance, T. R., Roberts, J. L., Plummer, C. T., Kiem, A. S., and van Ommen, T. D.: Interdecadal Pacific variability and eastern Australian megadroughts over the last millennium, Geophys. Res. Lett., 42, 129–137, doi:10.1002/2014GL062447, 2015.

Vance, T. R., Roberts, J. L., Moy, A. D., Curran, M. A. J., Tozer, C. R., Gallant, A. J. E., Abram, N. J., van Ommen, T. D., Young, D. A., Grima, C., Blankenship, D. D., and Siegert, M. J.: Optimal site selection for a high-resolution ice core record in East Antarctica, Clim. Past, 12, 595–610, doi:10.5194/cp-12-595-2016, 2016.

Verdon, D. C. and Franks, S. W.: Indian Ocean sea surface temperature variability and winter rainfall: eastern Australia, Water Resour. Res., 41, W09413, doi:10.1029/2004wr003845, 2005.

Verdon, D. C. and Franks, S. W.: Long-term behaviour of ENSO: interactions with the PDO over the past 400 years inferred from paleoclimate records, Geophys. Res. Lett., 33, L06712, doi:10.1029/2005GL025052, 2006.

Verdon, D. C. and Franks, S. W.: Long-term drought risk assessment in the Lachlan River Valley – a paleoclimate perspective, Australian J. Water Resour., 11, 145–152, 2007.

Verdon, D. C., Wyatt, A. M., Kiem, A. S., and Franks, S. W.: Multidecadal variability of rainfall and streamflow: eastern Australia, Water Resour. Res., 40, W10201, doi:10.1029/2004wr003234, 2004.

Verdon-Kidd, D. C. and Kiem, A. S.: Nature and causes of protracted droughts in southeast Australia: comparison between the Federation, WWII, and Big Dry droughts, Geophys. Res. Lett., 36, L22707, doi:10.1029/2009gl041067, 2009.

Verdon-Kidd, D. C. and Kiem, A. S.: Quantifying Drought Risk in a Nonstationary Climate, J. Hydrometeorol., 11, 1019–1031, doi:10.1175/2010jhm1215.1, 2010.

Whan, K., Timbal, B., and Lindesay, J.: Linear and nonlinear statistical analysis of the impact of sub-tropical ridge intensity and position on south-east Australian rainfall, Int. J. Climatol., doi:10.1002/joc.3689, 2013.